CONTACT METAMORHPISM OF THE MANCOS SHALE: IMPACTS ON SOLUTE RELEASE AND WEATHERABILITY IN THE EAST RIVER VALLEY, GOTHIC, CO

by

Bonnie C. Sams

A thesis submitted to the Faculty and the Board of Trustees of the Colorado School of Mines in partial fulfillment of the requirements for the degree of Master of Science (Hydrology).

Golden, Colorado

Date _____

Signed: _____

Bonnie Sams

Signed: _____

Dr. Alexis Navarre-Sitchler
Thesis Advisor

Golden, Colorado

Date _____

Signed: _____

Dr. Kamini Singha
Professor and Director
Hydrologic Science & Engineering Program

ABSTRACT

Alteration of rocks by contact metamorphism directly impacts rock pore structure and mineralogy, potentially decreasing weathering susceptibility and altering water residence times and release rates of aqueous solutes. Mountainous catchments, which can often be metamorphosed, are important for water and solute supply. Changes in the underlying lithology of a catchment can therefore directly impact water quality and solute release rates, imparting watershed scale changes in flow regimes and rate of flow within hydrologic systems. Here we aim to quantify differences in solute release rates from Mancos shale samples as a function of degree of metamorphism. Variable contact metamorphism of Mancos shale bedrock in the East River provides a natural test bed to investigate the role of underlying geology on weathering susceptibility, solute release rates and changing river chemistry in metamorphosed and unmetamorphosed sections of the Mancos shale.

To analyze the relationship between rate of solute release and degree of metamorphism, three trials of column scale experiments were conducted for unmetamorphosed and metamorphosed Mancos shale samples collected in the East River, Colorado. Steady state calcium release rates from metamorphosed samples were found to be an order of magnitude higher than the release of calcium from unmetamorphosed samples. These solute release rates will help constrain watershed scale weathering and solute sources in the East River to better understand the relationship between rates of rock weathering and catchment solute release. Different solute release rates calculated from metamorphosed and unmetamorphosed samples at the column scale can be used to further constrain the spatial variation of weatherablity in metamorphosed and unmetamorphosed shale. Changes in release rates from unmetamorphosed and metamorphosed samples could be linked to differences present in sample mineralogy.

TABLE OF CONTENTS

LIST OF FIGURES

LIST OF TABLES

ACKNOWLEDGEMENTS

This work would not have been possible without the Department of Energy, the Rocky Mountain Biological Laboratory, the Colorado School of Mines and my advisor, Dr. Alexis Navarre-Sitchler. A special thank you also goes to my committee members, Dr. Kamini Singha and Dr. James Ranville, for all of their time and effort in reviewing and discussing this work.

This work is dedicated to my late father, James Richards Sams, who would be incredibly proud of the passion and devotion I have put into my research, and whose love and encouragement always served as my guiding light.

CHAPTER 1

GENERAL INTRODUCTION

High elevation catchments are sensitive indicators of climate change (Winnick et al., 2017). Freshwater solute supply in mountainous watersheds is stored as winter snowpack and released as snowmelt, making alpine catchments important sources of water for much of the western United States (Winnick et al., 2017). High elevation sedimentary hosted catchments often exhibit lithologic heterogeneities or undergo contact metamorphism, altering the weathering and solute release rates for freshwater systems. The release of solutes into hydrologic systems is controlled by water-rock interactions and rock weathering processes.

The controlling factors behind rock weathering processes have been studied extensively for a number of decades (Maher, 2010). The nature of underlying lithology plays a major role in dictating flow regimes and rate of flow through porous media within hydrologic systems, and lithologic heterogeneities complicate our understanding of rock weathering processes. Alteration of rocks by metamorphism directly impacts rock pore structure, changing the nature of water movement in porous media and imparting changes in rock weathering susceptibility (Maher, 2011; Li et al., 2016). Changes in fluid pathways and residence time associated with metamorphism correspond to differences in solute release rates and changing river chemistry (Li et al., 2016; Maher, 2011).

There are very few studies of the role that lithologic heterogeneity plays in the spatial distribution of solute release rates in mountainous watersheds (Gaillardet et al., 1999). In this study, we quantify differences in solute release rates from samples of a variably metamorphosed, shale-hosted watershed in the Rocky Mountains of Colorado. The East River is headwater, high elevation watershed located in the Colorado River drainage network adjacent to Mount Crested

Butte in the West Elk Mountain Range in southern central Colorado. In the upper reaches of the river, contact metamorphism by Tertiary aged volcanic intrusions has variably altered the surrounding sedimentary rock, including the Cretaceous Mancos shale that is the predominant bedrock unit underlying the East River. Variable contact metamorphism of Mancos shale bedrock in the East River provides a natural test bed to investigate the role of lithologic variability induced by contact metamorphism of shales on weathering susceptibility and solute release rates at the watershed scale.

CHAPTER 2

CONTACT METAMORHPISM OF THE MANCOS SHALE: IMPACTS ON SOLUTE RELEASE AND WEATHERABILITY IN THE EAST RIVER VALLEY, GOTHIC, CO

A paper to be submitted to *the Journal of Chemical Geology*

Bonnie Sams[1], Rania Pommer[2], Alexis Navarre-Sitchler[1,2*]

2.1 Abstract

Alteration of rocks by contact metamorphism directly impacts rock pore structure and mineralogy, potentially decreasing weathering susceptibility and altering water residence times and release rates of aqueous solutes. Mountainous catchments, which can often be metamorphosed, are important for water and solute supply. Changes in the underlying lithology of a catchment can therefore directly impact water quality and solute release rates, imparting watershed scale changes in flow regimes and rate of flow within hydrologic systems. Here we aim to quantify differences in solute release rates from Mancos shale samples as a function of degree of metamorphism. Variable contact metamorphism of Mancos shale bedrock in the East River provides a natural test bed to investigate the role of underlying geology on weathering susceptibility, solute release rates and changing river chemistry in metamorphosed and unmetamorphosed sections of the Mancos shale.

[1]Hydrologic Science and Engineering, Colorado School of Mines
[2]Departement of Geology and Geological Engineering, Colorado School of Mines
[*]Corresponding author: asitchle@mines.edu

To analyze the relationship between rate of solute release and degree of metamorphism, three trials of column scale experiments were conducted for unmetamorphosed and metamorphosed Mancos shale samples collected in the East River, Colorado. Steady state calcium release rates from metamorphosed samples were found to be an order of magnitude higher than calcium release from unmetamorphosed samples. The relationship between the weathering of rocks and water chemistry within a catchment has been the focus of previous studies (Horton et al., 1999; Gailardet et al., 1999). These solute release rates will help constrain watershed scale weathering and solute sources in the East River to better understand the relationship between rates of rock weathering and catchment solute release. Different solute release rates calculated from metamorphosed and unmetamorphosed samples at the column scale can be used to further constrain the spatial variation of weatherablity in metamorphosed and unmetamorphosed shale.

2.2 Introduction

Fine-grained shales and laminated sedimentary rocks make up approximately two thirds of all rocks in the Earth's crust and 25.4% of all rocks exposed at the continental surface (Suchet et al. 2003; Rimsdtidt, 2017; Hidaglo, 2001; Ilgen et al, 2017). Shales play a crucial role in many natural processes and are important in fluid-rock interactions at the earth’s surface and in the shallow subsurface, making water-shale interactions important in fresh water solute supply and nutrient cycling (Price, 2004; Milliken, 2004; Illgen et al., 2017). Shale samples are polymineralic by nature, making their dissolution and weathering processes more complex than those of pure minerals.

While the unique and heterogeneous physical characteristics of shale have made them heavily studied (e.g. Illgen et al., 2017), knowledge of shale heterogeneity in chemistry, mineralogy and pore structure is far from complete (Bernard et al., 2012; Chen et al., 2014). Fine

grained sedimentary rocks like shale have been shown to display heterogeneity on submillimeter to centimeter scale (Illgen et al., 2017). Though shale weathering has been the focus of many studies, quantitative models to predict rates of shale weathering are still unavailable (Jin L, 2010; Liermann et al., 2011; Jin L 2014; Ma L et al., 2015; Rimstidt et al., 2017). Physical and chemical changes in shale mineralogy affect the rate of chemical reactions in natural porous media (Hunt et al., 2015; Heidari et al. 2017). It is also well known that the lithologic heterogeneities prevalent in shales can cause spatially variable geochemical reactive transport conditions at the watershed scale (van der Zee and van Remsdijk, 1991; Barber et al., 1992; Atchley et al., 2014), ultimately impacting the spatial distribution of solute release within a watershed.

In addition to the heterogeneity in shales related to depositional and diagenetic processes, shales in mountainous regions can also be subjected to pressure and temperature conditions that induce further changes related to metamorphism. Contact metamorphism related to igneous intrusions in sedimentary basins will produce variations in rock properties, such as mineralogy, organic geochemistry, and rock microstructure (Senger et al., 2014; Li et al., 2016; Illgen et al., 2017). These changes in rock pore structure and mineralogy can decrease weathering susceptibility and alter the residence times and release rates of aqueous solutes (e.g. Anovitz, 2009).

To study the effects of lithologic variation and contact metamorphism of shales on weatherablity and solute-release potential, we collected samples from the East River watershed, a mountainous, high elevation sedimentary-rock hosted catchment located adjacent to Mount Crested Butte in the West Elk Mountain Range in southern central Colorado (Figure 1). The dominant bedrock unit underlying the East River is the Mancos shale, a Cretaceous, carbon-rich marine unit that is extensively present in much of the western United States (Nadeau et al., 1981). In the upper reaches of the East River, contact metamorphism by tertiary-aged volcanic intrusions

has variably altered the Mancos Shale, imparting changes in lithology throughout the East River valley (Rania Eldam Pommer and Navarre-Sitchler, in prep).

Weathering is likely an important source of shale weathering derived solutes in the East River, thus, quantifying solute release rates as a function of degree of metamorphism will help elucidate the spatial variability of weathering and constrain overall weathering solute production in the at the watershed scale. Here we quantify release rates of calcium, magnesium and silica from metamorphosed and unmetamorphosed Mancos shale using four samples (two metamorphosed and two unmetamorphosed) collected from the East River watershed. Column experiments were performed at varying flow rates to ensure solute release rates are not controlled by transport conditions in the column

2.3 Methods

Methods are presented in the following section for sample collection and laboratory analysis.

2.3.1 Sample Collection and Preparation

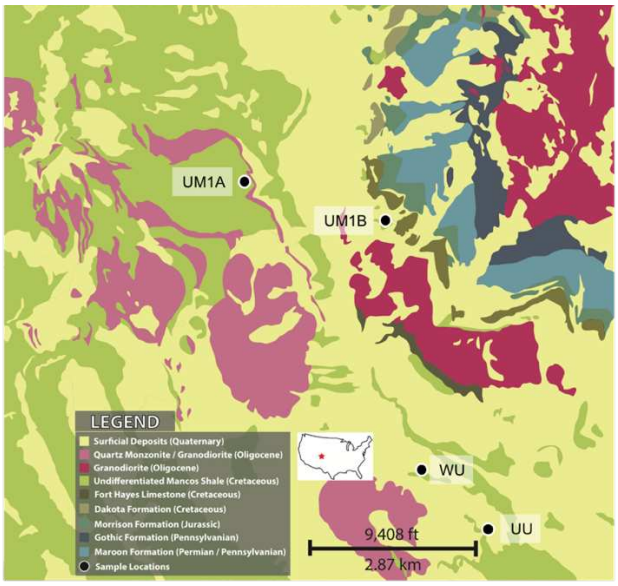

Figure 2.1. Map of the East River Watershed area, showing geologic formations and metamorphosed and unmetamorphosed sampling locations.

In the upper reaches of the East River valley, variable contact metamorphism of the Mancos shale has altered the bedrock underlying the riverbed, producing steep banks and straight narrow channels. Weathered and unweathered samples of unmetamorphosed Mancos (WU and UU respectively) were taken from outcrops the lower reaches of the East River watershed, where the river banks and bed are wide and meandering. Unweathered, unmetamorphosed samples were taken from a sheltered outcrop (figure 1) while weathered samples were taken from a weathered, in place bed of Mancos shale. Two metamorphosed samples (denoted UM1A and UM1B, Figure 1) were collected from the upper reaches of the field site, in close proximity to tertiary aged granitic intrusions.

After collection, all samples were crushed to a median size of approximately 2.5 x 2.5 cm to expose fresh surface area and minimize differences in size of column packing material. Crushed samples were then placed in Nalgene bottles with deionized water in an ultrasonicator bath for five minutes, the fluid was decanted to remove fines, and the samples were oven dried at 50°C for 48 hours.

2.3.2 Column Experiments

Column experiments were performed at ambient temperatures of ~ 20°C in clear acrylic polycarbonate columns with an internal diameter of 5.08 cm. Initial columns were 0.6 meters in length, this was reduced after several column experiments to 0.3 meters to reduce the sample sizes and water volumes necessary for the column experiments. Input fluid was comprised of a synthetic rainwater composition with conductivity ranging from 20-25 μS/cm and pH ranging from 5.4 to 5.6 (Davies, 2004). Amount of inorganic salts per 1 liter of DI water used in the synthetic rainwater solution are reported in Table 1. Sodium azide at a concentration of 0.05% by volume was added to the input solution to prevent bacterial growth (Neaman et al, 2004).

A Fisher Scientific™ FH100 peristaltic pump was used to pump the synthetic rainwater at fixed flow rates of 1mL min^{-1} or 2mL min^{-1} into the columns with flow from the bottom to the top (Figure 2). The influent and effluent tubing was constructed of Thermo Scientific™ All-Purpose Tubing size 14. All column bases were constructed using PVC tubing caps and quartz fritted discs were placed at the bottom and top of the columns to disperse flow into the column and filter any fine material. Columns were mounted vertically on ring stands and shielded from incoming sunlight to minimize temperature fluctuations.

Table 2.1. Inorganic salts used in synthetic rainwater solution. Inorganic salts adapted from methods in Davies, 2011.

Inorganic Salt	Weight [mg/L DI]
$NaNO_3$	4.07
KCl	0.35
$CaCl_2 \bullet 2H_2O$	3.24
$MgSO_4 \bullet 7H_2O$	2.98
$(NH_4)_2SO_4$	2.41

After attaching the column base, Mancos shale samples were wet-packed into columns incrementally. Column packing material was added in 0.2 to 0.3 kg increments. Input solution was added and the column material was shaken and stirred to ensure equal distribution of packing material. A control column was conducted with no rock to quantify elemental release from column materials and concentrations of input solution were measured for each experimental run (Table 2). All column scale experiments were conducted in triplicate with new columns manufactured for each.

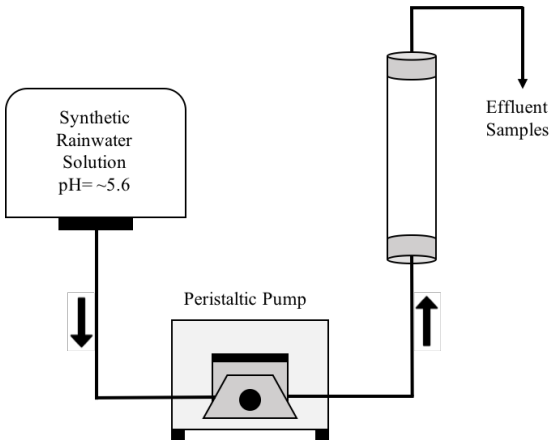

Figure 2.2. Schematic of the flow-through column scale experimental set up for studying solute release rates as a function of mineralogy and degree of metamorphism.

Table 2.2. Input solution concentrations from ICP-AES analysis subtracted from effluent column concentrations used in release rates

Analyte	Concentration (mg/L)
Ca	0.45
Mg	0.27
Si	0.72

2.3.4 Pore Volume Calculations

The porosity (η) of each column was calculated using equation 1, where M_w (g) is the mass of water in the column determined by the difference in mass between a saturated and dry column, V_T (cm^3) is the total volume of the column (calculated as $\pi r^2 h$ with r = 5.08 cm and h = 0.3 or 0.6 m, and ρ_w is the density of water (1 g cm^{-3}).

$$\eta = \frac{M_w}{V_T \rho_w} \tag{2.1}$$

Data were analyzed as a function of pore volumes, not absolute time, to compare data from columns with different flow rates. The number of pore volumes that flowed through the column at a given time (P_t) was calculated using equation 2.

$$P_t = \frac{\eta V_T \rho_w}{q} \quad (2.2)$$

Where t is the time of sampling (in minutes from start of the experiment), and q is the volumetric flow rate of water pumped into the column (mL min^{-1}). Experimental conditions for each column replicate are shown in Table 3.

Table 2.3. Sample descriptions and parameters for all individual column experiments.

	Sample Description	Flow Rate (mL min^{-1})	Porosity (η)	Residence Time (hours) *	Total kg of Rock
Unmetamorphosed					
$UU1_1$	unweathered, unmet.	1.0	0.52	10.4	1.4
$UU1_2$	unweathered, unmet.	1.0	0.55	9.6	1.4
$UU1_3$	unweathered, unmet.	1.0	0.51	9.05	1.8
$WU1_1$	weathered, unmet.	1.0	0.61	13.0	1.3
$WU1_2$	weathered, unmet.	1.0	0.51	5.0	1.4
$WU1_3$	weathered, unmet.	1.0	0.51	8.5	2.1
Unmetamorphosed					
$UU2_1$	unweathered, unmet.	2.0	0.51	4.3	1.4
$UU2_2$	unweathered, unmet.	2.0	0.83	4.3	0.64
$UU2_3$	unweathered, unmet.	2.0	0.74	3.8	0.69
$WU2_1$	weathered, unmet.	2.0	0.84	5.0	1.3
$WU2_2$	weathered, unmet.	2.0	0.65	2.8	0.55
$WU2_3$	weathered, unmet.	2.0	0.72	2.3	0.52
Metamorphosed					
$UM1A_1$	Near Mt. Gothic	1.0	0.86	9.5	1.4
$UM1A_2$	Near Mt. Gothic	1.0	0.78	9.9	1.1
$UM1A_3$	Near Mt. Gothic	1.0	0.49	8.2	2.0
$UM1B_1$	Near Copper Creek Sill	1.0	0.57	10.0	1.8
$UM1B_2$	Near Copper Creek Sill	1.0	0.63	5.4	0.70
$UM1B_3$	Near Copper Creek Sill	1.00	0.64	5.4	0.69

** Cap volume not accounted for in porosity calculations, which can impact residence time calculations. A propagated error of roughly 10% is assumed.*

2.3.5 Experimental Analysis

Samples were collected from the column in roughly 40 mL amounts at approximately 24-hour intervals and input solution samples were collected before the start of each column trial. All samples were filtered to 0.45 μm with a nylon filter. 1% HNO_3 (nitric acid) was used to acidify

samples for cation analysis using ICP-AES analysis (raw data in appendix 1). Na was not included in analytes of interest due to the addition of Na-azide to prevent bacterial growth

Fresh samples were measured for C and N by high-temperature combustion at the USGS laboratories in Denver, Colorado. Samples were sieved to 2.5 cm and then a mortar and pestle were used to grind samples until they completely passed an 80 μm sieve. Sieved samples were then weighed into tin capsules and analyzed using a Carlo Erba NA1500 elemental analyzer (CE Elantech Inc., Lakewood, NJ1).

Mineral assemblages were analyzed using X-Ray Diffraction, scanning electron microscopy (SEM) and examination of thin sections under a petrographic microscope. Fresh samples not used in columns and reacted samples from selected column experiments were analyzed using scanning electron microscopy (SEM, HITACHI TM-3000) for evidence of weathering after column experiments were run. Images of carbon coated samples were taken at an accelerating voltage of 15 kV and varying magnification.

X-ray diffraction data were collected from whole rock samples, clay separates, and ethylene glycol desiccated clay separates for mineral identification according to methods from Moore and Reynolds (1989) and Brindley and Brown (1980). Briefly, samples were crushed to < 0.2 mm grain size. Random powder mounts were analyzed from 4° to 65° 2θ at a continuous scan rate of 2.0°/minute. The Millipore method (Moore and Reynolds, 1989) was used to obtain a < 2 μm clay fraction from all samples. Clay fractions prior to and after ethylene glycol treatment were analyzed from 2° - 40° 2θ at a continuous scan rate of 1.50°/minute.

2.3.6 Surface Area and Mass Normalized Solute Release Rates

Bulk mass release rates (mole sec^{-1}) were calculated using equation 3, where q is the flow rate in liters per second, $C_{in,x}$ corresponds to the input concentration for a solute of interest x and

$C_{out,x}$ corresponds to the effluent concentration of that solute.

$$R_x = q[C_{out,x} - C_{in,x}] \quad (2.3)$$

Solute release rates for each Mancos shale sample used in this study were normalized to surface areas measured with the Brunauer, Emmett and Teller modeled N_2 gas sorption isotherms (BET). Surface area normalization is typical because weathering is proportional to the reactive surface area defined as the density of reactive sites on a silicate surface at which hydrolysis reactions occur (Brunauer et al., 1938; Brantley et al., 2005; Hodson, 2006). Steady state effluent concentrations were normalized to BET surface area (mole m^{-2} sec^{-1}) using equation 4, where R_x is the bulk release rate from equation 3, M_R is the mass of rock in the column in kilograms and S_{BET} is the BET surface area (m^2 g^{-1}) of a given sample (Table 4).

$$R_{BETx} = \frac{R_x}{S_{BET}} M_R \quad (2.4)$$

Because of discrepancies surrounding BET normalized release rates (Brantley et al., 2008), effluent solute concentrations were also normalized to the total mass of rock in each column (mole kg^{-1} sec^{-1}) using equation 5 (Table 4).

$$R_{Mx} = \frac{R_x}{M_R} \quad (2.5)$$

2.3.7 Steady State Analysis

Mass and BET normalized molar release rates of Ca, Si, and Mg were calculated from the column after steady-state effluent concentrations were reached using equations 4 and 5. Steady state was determined by taking the first derivative of each solute concentration (in mg/l) and plotting against pore volumes. For this study, steady state is defined as the point at which half of more of the derivatives of concentration fall between 1 and -1 mg/L. Steady state estimations for

individual replicate experiments were made using the last three release rates from each individual trial to generate a steady state value for each experiment. The last three release rates for each column were averaged together, producing average release for each column replicate. Finally, average steady state release values from each replicate were averaged together, producing steady state estimations for each rock type and flow condition.

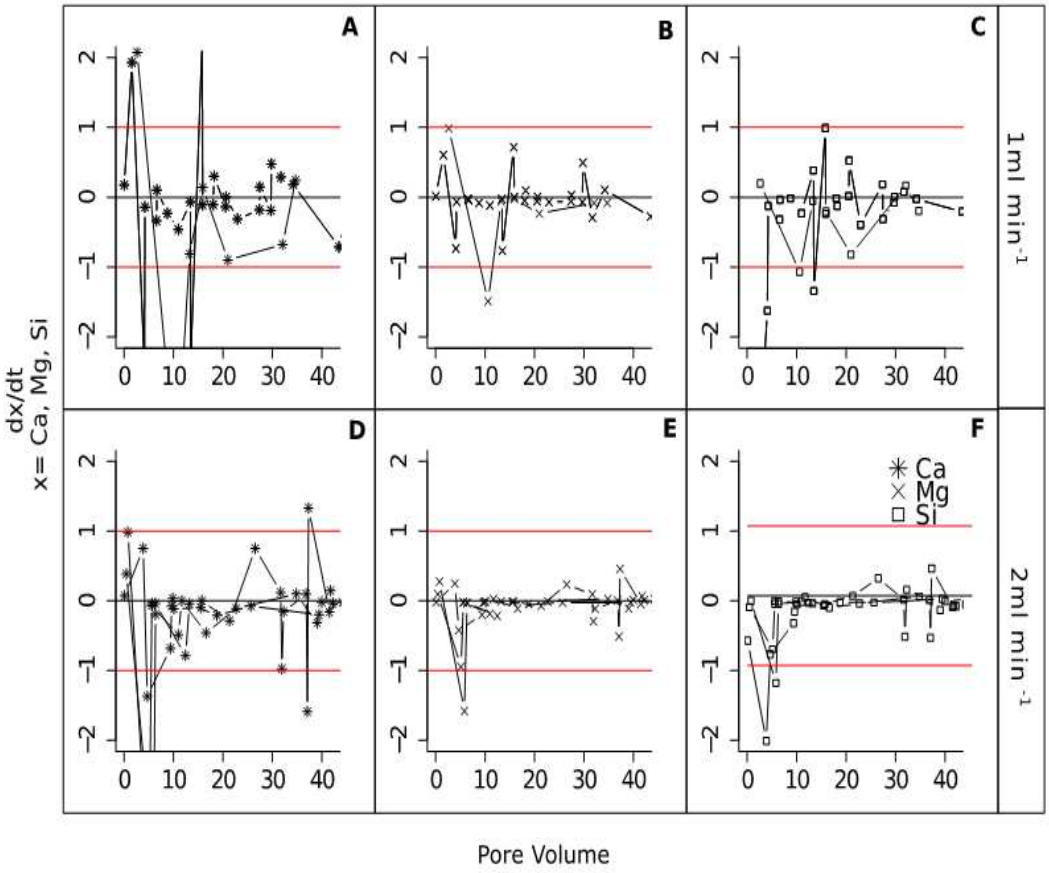

Figure 2.3. Steady state estimations for all trials of unweathered unmetamorphosed UU at 1 mL min^{-1} (A, B and C respectively) and at 2 mL min^{-1} (D, E and F respectively). Steady state change in concentration in mg/L for Calcium, Magnesium and Silica are reported for each UU sample at each flow condition.

2.3.8 Statistical Methods

To determine if steady state values from replicate column experiments of the same material and flow condition were from the same population, the nonparametric Kruskal-Wallis test was used to analyze for statistically significant differences between each column replicate. Kruskal-Wallis testing was carried out to compare steady state release rates of calcium, magnesium and silica release from columns of the same material, at the same flow rate to see if they are from the same population. To analyze statistical differences between release rates of calcium, magnesium and silica in columns from different experiments, the Friedman test was employed to test for differences between groups with ordinal steady state values of solutes.

In the calculation of steady state release rates, the last three values from each trial were averaged together to produce one steady state value for each replicate column experiment. Error was accounted for by taking the standard deviation of the three replicate steady state values divided by the square-root of the number of points averaged (Tellinghuisen, 2001). This is shown using equation 6, where ε_x is the resulting error for a solute of interest (x), σ is the sample standard deviation and n is the total number of points averaged.

$$\varepsilon_x = \frac{\sigma}{\sqrt{n}} \tag{2.6}$$

The sample standard deviation was found using equation 7 where X_i is the value of each point in the data set and $\overline{X}$ is the average value for the data set.

$$\sigma = \sqrt{\frac{1}{n-1}\sum_{i=1}^{n}(X_i - \overline{X})^2} \tag{2.7}$$

2.4 Results

Results are presented in the following section by analysis and then by column type.

2.4.1 Sample Characterization

In Table 4, XRD bulk rock analysis results are reported for each of the four samples used in this study. Mineralogy is variable in the samples selected with quartz and calcite comprising the majority of the unweathered samples and feldspar and clay as minor constituents (Table 4). In the weathered sample clay comprised 38% of the sample by weight. A comparison of unmetamorphosed samples UU and WU shows that they exhibit compositional differences, particularly for quartz and clay content. Metamorphosed samples UM1A and UM1B have clay composition comparable to that of sample UU, but both metamorphosed samples have higher carbonate mineral content.

Table 2.4. XRD bulk rock analysis results, BET surface area results and TC results are reported for each of the four samples used in this study.

Sample ID	% Quartz	% Feldspar	% Clay	%Carbonate	B.E.T m^2/g	TC %
UU	70	14	9	7	11.9	1.3
WU	49	7	38	6	20.4	7.4
UMA	46	0	12	42	5.01	8.5
UMB	34	0	10	56	1.2	10.1

2.4.2 Solute Release Rates

To analyze the relationship between solute release rates and rate of fluid flow, two experimental flow conditions were implemented for both unmetamorphosed samples. Metamorphosed column experiments were conducted at a flow rate of 1 mL min^{-1}. Figure 4 shows average mass normalized steady state release rates for all columns at all flow conditions with vertical error bars. R_{Mg} and R_{Si} were highest in metamorphosed sample UM1A (figure 4). R_{Ca} is

highest from UM1B. A comparison of both metamorphosed samples UM1A and UM1B show different rates of release for all solutes measured for both metamorphosed samples.

Table 2.5. Steady state release rates in mole/second for all column experiments.

R_{Mx}	UU1	WU1	UU2	WU2	UM1A	UM1B
$[Ca^{2+}]$	7.4×10^{-05}	9.8×10^{-05}	3.6×10^{-05}	1.2×10^{-04}	1.2×10^{-04}	9.4×10^{-05}
$[Mg^{2+}]$	2.4×10^{-05}	2.8×10^{-05}	1.8×10^{-06}	1.4×10^{-05}	2.3×10^{-05}	2.3×10^{-06}
$[Si^{2+}]$	3.1×10^{-05}	3.2×10^{-05}	7.2×10^{-06}	1.2×10^{-05}	7.1×10^{-05}	1.3×10^{-05}

Release rates of calcium from UU1 and WU1 are within the same order of magnitude at the slower flow rates (1 ml min^{-1}). At the faster flow rates (UU2 and WU2 at 2 ml min^{-1}) release rates are different by an order of magnitude. Order of magnitude differences in the release rate of solutes are present comparing UU1 and WU1, but not for those samples at fast flow conditions (UU2 and WU2). Specifically in the case of sample UU, R_{Si} and R_{Mg} release rates decrease by an order of magnitude for fast flow conditions. Order of magnitude differences are also present in both unmetamorphosed Mancos shale samples at low flow conditions compared to those samples at 2 mL min^{-1} flow rates. These differences indicate that calcium release, potentially due to calcite dissolution, could be sensitive to changes in flow rate and that flow rate impacts release rates from column to column. Differences in ratios of Ca^{2+}/Mg^{2+} could indicate that calcite dissolution is transport limited due to calcite dissolution at faster flow rates producing higher Ca^{2+}/Mg^{2+} ratios.

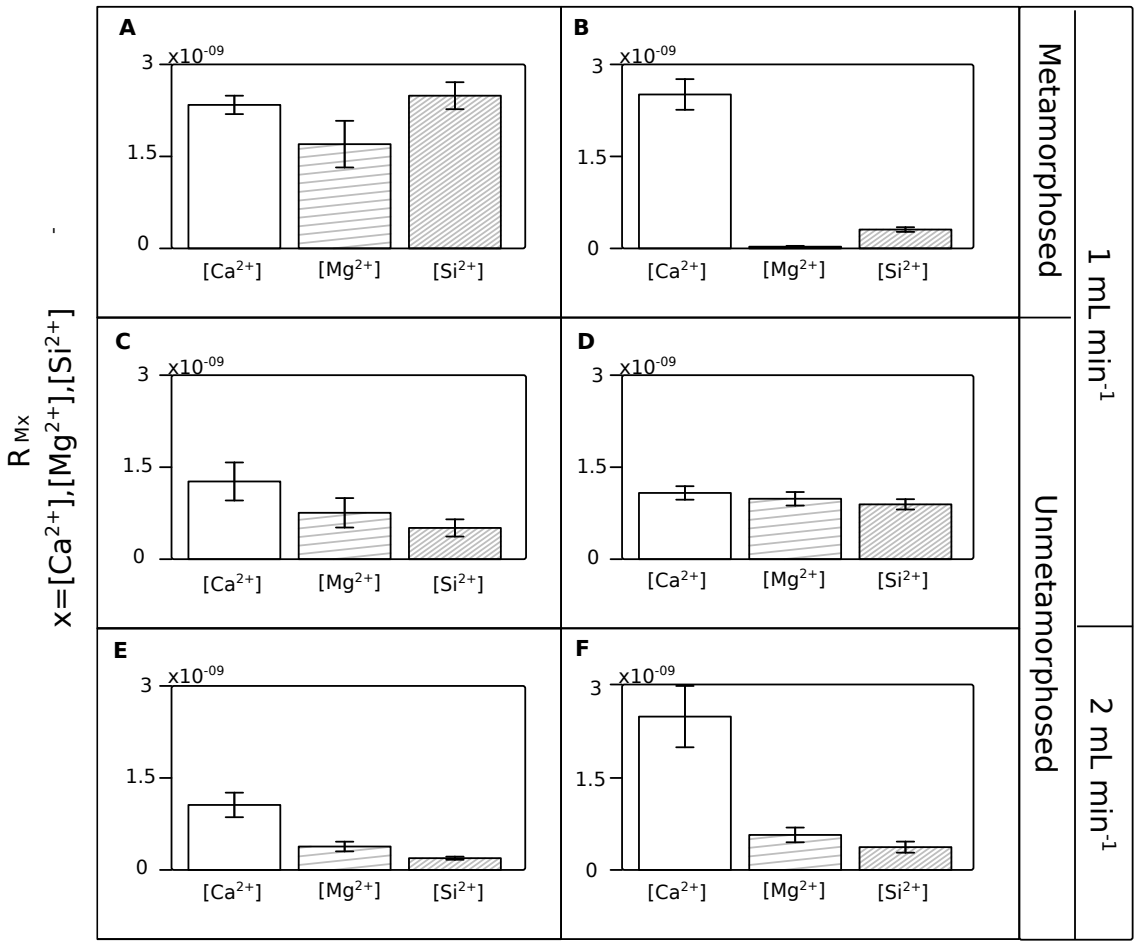

Figure 2.4. Summary figure showing average steady state mass normalized release rates for all columns at all flow conditions. Metamorphosed samples UM1A and UM1B are shown on the top row in subfigures A and B respectively. Samples UU and WU at 1 mL min^{-1} are shown in C and D respectively, with UU2 and WU2 at 2 mL min^{-1} shown in subfigures E and F.

Table 2.6. Values for average mass normalized steady state release rates for all column experiments.

	R_{Mx}			Error ε_x		
	$[Ca^{2+}]$	$[Mg^{2+}]$	$[Si^{2+}]$	$\varepsilon[Ca^{2+}]$	$\varepsilon[Mg^{2+}]$	$\varepsilon[Si^{2+}]$
UU1	1.3×10^{-09}	2.3×10^{-10}	1.2×10^{-10}	$\pm 3.1 \times 10^{-10}$	$\pm 2.4 \times 10^{-10}$	$\pm 1.4 \times 10^{-10}$
WU1	1.9×10^{-09}	1.5×10^{-10}	8.9×10^{-10}	$\pm 1.1 \times 10^{-10}$	$\pm 1.1 \times 10^{-10}$	$\pm 8.4 \times 10^{-11}$
UU2	3.7×10^{-10}	3.8×10^{-10}	1.6×10^{-10}	$\pm 2.0 \times 10^{-10}$	$\pm 7.9 \times 10^{-11}$	$\pm 2.5 \times 10^{-11}$
WU2	5.2×10^{-10}	3.9×10^{-10}	3.4×10^{-10}	$\pm 5.0 \times 10^{-10}$	$\pm 1.2 \times 10^{-10}$	$\pm 9.0 \times 10^{-11}$
UM1A	1.9×10^{-09}	6.7×10^{-10}	8.7×10^{-10}	$\pm 1.5 \times 10^{-10}$	$\pm 3.8 \times 10^{-10}$	$\pm 2.2 \times 10^{-10}$
UM1B	1.7×10^{-09}	3.7×10^{-11}	2.1×10^{-10}	$\pm 2.5 \times 10^{-10}$	$\pm 1.3 \times 10^{-11}$	$\pm 3.8 \times 10^{-11}$

2.4.3 Unweathered, Unmetamorphosed: UU

Steady state mass release rates for all column replicates of sample UU are reported in Table 7 for both flow conditions. The relationship between flow rate and rate of chemical weathering has been explored in a number of studies and was found to vary with mineralogy and laboratory setting (Velbel, 1993; Clow and Drever, 1996; Blum et al., 1998). Here, release rates have been observed to be controlled heavily by mineralogy and laboratory flow condition. Statistical analysis of steady state mass normalized release rates from UU samples at both flow conditions were carried using Kruskal-Wallis nonparametric testing. When comparing release rates of R_{Ca}, R_{Mg} and R_{Si} for all column replicates of UU1 and UU2, significant p values were found, indicating that all replicate values for both UU1 and UU2 trials are statistically similar ($p >> 0.05$).

Table 2.7. Steady state average mass normalized release rates from all columns of UU and WU at both flow conditions. Highest release rates of any solute in all trials are seen for calcium.

R_{Mx}	$UU1_1$	$UU1_2$	$UU1_3$	$UU2_1$	$UU2_2$	$UU2_3$
$[Ca^{2+}]$	5.0×10^{-10}	2.5×10^{-09}	8.2×10^{-10}	2.7×10^{-10}	1.3×10^{-09}	1.6×10^{-09}
$[Mg^{2+}]$	2.0×10^{-10}	1.7×10^{-09}	3.7×10^{-10}	9.4×10^{-11}	4.2×10^{-09}	6.3×10^{-09}
$[Si^{2+}]$	8.7×10^{-11}	9.4×10^{-09}	6.8×10^{-10}	1.4×10^{-10}	1.9×10^{-09}	2.5×10^{-09}
R_{Mx}	$WU1_1$	$WU1_2$	$WU1_3$	$WU2_1$	$WU2_2$	$WU2_3$
$[Ca^{2+}]$	2.0×10^{-09}	1.3×10^{-09}	1.7×10^{-09}	5.2×10^{-10}	3.4×10^{-09}	3.6×10^{-09}
$[Mg^{2+}]$	1.2×10^{-09}	1.1×10^{-09}	7.1×10^{-10}	3.9×10^{-10}	1.0×10^{-09}	2.9×10^{-10}
$[Si^{2+}]$	1.1×10^{-09}	5.8×10^{-10}	1.0×10^{-09}	8.0×10^{-11}	3.4×10^{-10}	6.9×10^{-10}

2.4.4 Weathered Unmetamorphosed: WU

Steady state release rates for all flow conditions are reported in Table 7 for weathered, unmetamorphosed (WU) columns. When comparing R_{Ca}, R_{Mg}, and R_{Si} for all column replicates of WU1 and WU2 using a Kruskal-Wallis test, significant p values were found, indicating that all column trials of the same material or flow rate are from the same population.

2.5.1 Sample Mineralogy

Both weathered and unweathered unmetamorphosed Mancos shale exhibit similar trends in bulk solute release rates, with $R_{Ca} > R_{Mg} > R_{Si}$ for both UU and WU at both flow conditions. Order of magnitude differences in release rate of solutes are present comparing UU1 and WU1, WU1 and WU2 but not for those samples at fast flow conditions (UU2 and WU2). Order of magnitude differences present in weathered unmetamorphosed Mancos shale sample WU at different flow conditions indicate that calcium release, potentially due to calcite dissolution, could be sensitive to changes in flow rate. Order of magnitude differences are also present for unweathered unmetamorphosed sample UU for all solutes at different flow conditions, indicating that flow rate impacts release rates from column to column. Specifically for sample UU, magnesium and silica release rates decrease by an order of magnitude for fast flow conditions.

2.5.2 Changes in Mineralogy from Contact Metamorphism

Contact metamorphism of the shales by granitic intrusion triggers the thermal reaction of organics, filling the macropores and microcracks of metamorphosed shales with microcrystalline quartz, ultimately decreasing the BET surface area and porosity of shales near igneous intrusions

(Li et al., 2016). When coupled with changes in weatherablity, changes in the mineral composition of metamorphosed sedimentary rocks have the potential to produce differences in solute release rates of more highly metamorphosed samples. Proximity from tertiary aged volcanic intrusions plays a large part in sample mineralogy and chemical weathering rates. In analysis of metamorphic samples (UM1A and UM1B), relative location to metamorphic aureoles, XRD data shows a decrease in clay composition for both metamorphic samples.

Contact metamorphism has altered the nature of solute release in both metamorphosed Mancos shale samples. Calcium release was highest for both metamorphosed columns, followed by the steady state release of silica. Metamorphosed Sample UM1B exhibited the highest steady state calcium release for any column trial, while sample UM1A, taken from the base of Mt. Gothic (seen in figure 1) was observed to have the highest rate of release for Mg, Si and Sulfate for any column trial. A direct comparison of both metamorphosed samples shows that the release of solutes at steady state from UM1A and UM1B are drastically different (figure 4, subfigures A and B respectively). Order of magnitude differences in the steady state release of solutes from UM1A and UM1B is controlled by the spatial distribution of contact metamorphism within the Mancos shale unit.

2.5.3 BET and Mass Normalized Solute Release Rates

The use of different normalizing terms in previous studies of mineral dissolution rates have been shown to yield different estimates of the physical surface area of mineral grains (Anbeek, 1992; Drever, 1993). It is well established that not all mineral surfaces dissolve at the same rate (Lee et al., 1998; Hodson, 2006) and that potential surface area available for dissolution does not scale linearly with mass (Hodson, 2006).

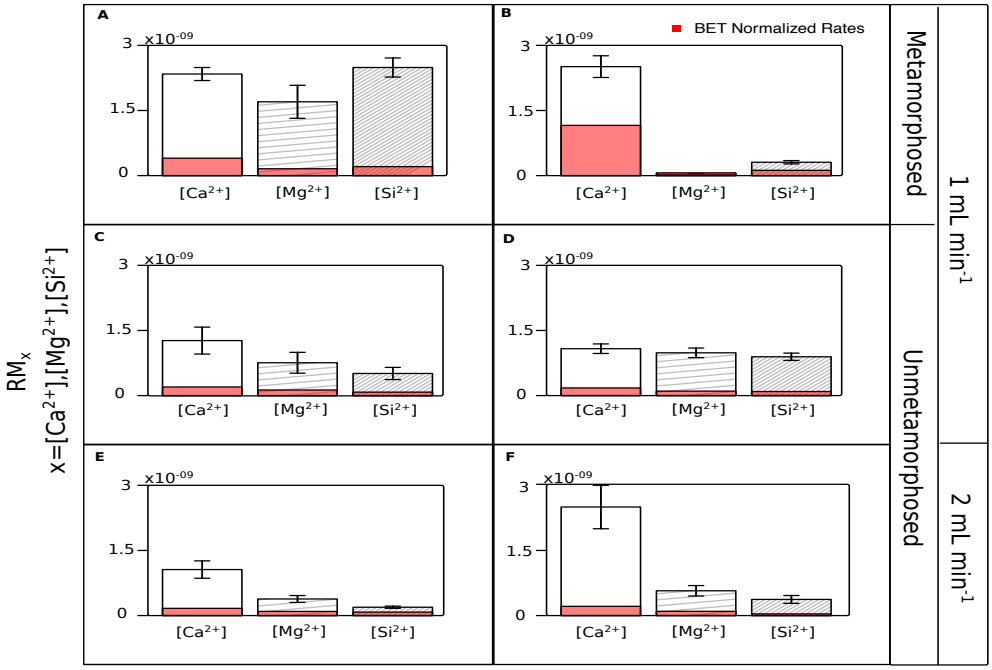

Figure 2.5. A comparison of mass normalized and BET normalized steady state release rates for Ca, Mg, Si.

In this study, steady state release rates of selected solutes were normalized to both mass of rock in each column and BET surface area for comparison (figure 5). On average, BET normalized release rates are lower than release rates normalized to only the mass of the column. The largest differences between rates are seen for calcium release, where mass normalized steady state release of calcium for all unmetamorphosed columns at 1 mL min^{-1} and both metamorphosed samples UM1A and UM1B are significantly larger than BET rates.

Table 2.8. BET normalized average steady state release rates for all column trials at all flow conditions.

R_{BETx}	UU1	WU1	UU2	WU2	UM1A	UM1B
$[Ca^{2+}]$	1.0×10^{-10}	2.2×10^{-11}	3.1×10^{-11}	2.6×10^{-11}	3.3×10^{-10}	8.7×10^{-10}
$[Mg^{2+}]$	1.9×10^{-11}	7.3×10^{-12}	3.2×10^{-11}	1.9×10^{-11}	1.2×10^{-10}	1.9×10^{-11}
$[Si^{2+}]$	1.0×10^{-11}	4.4×10^{-11}	1.3×10^{-11}	1.7×10^{-11}	1.5×10^{-10}	1.1×10^{-10}

2.6 Conclusions

Here we have utilized methods for mineral weathering at the column scale and applied it to whole rock weathering in shales as a means to understand how lithologic heterogeneities impact watershed-scale behaviors. The integration of small-scale, subsurface heterogeneities with changes in watershed scale processes is crucial in developing accurate models and furthering our knowledge of how shale dominated watershed weather. Changes in underlying lithology impact large scale watershed processes and ultimately produce different weathering rates for localized areas within a single watershed. Ultimately, weathering susceptibility and rate of solute release is a function of mineralogy, which has been shown here to be impacted by extent of metamorphism and rock mineral composition.

For all column trials at all flow conditions, steady state release of calcium (R_{Ca}) is always the highest observed release rate when compared to other solutes of interest and appears to be correlated to the calcite content of the sample. Metamorphosed samples contained on average 42% more calcite than unmetamorphosed samples and exhibited higher release rates of calcium than unmetamorphosed samples by an order of magnitude.

Trends in solute release from both metamorphosed samples UM1A and UM1B have the same trend in rates of release where $R_{Ca} > R_{Si} > R_{Mg}$. The trend in the rate of solute release from unmetamorphosed columns was the same for each sample type with $R_{Ca} > R_{Mg} > R_{Si}$. Differences in the rate of release from the two unmetamorphosed samples (UU and WU) and metamorphosed samples A and B correlate with mineralogical similarities between metamorphosed and unmetamorphosed sample groups.

Weathering susceptibility and rate of solute release within a catchment is a function of mineralogy. The characteristics of mineral distribution patterns and overall mineral composition

have been shown to determine the extent water–rock interactions within a watershed (F. Salehikhoo, et al., 2015). XRD bulk rock analysis results in Table 3 show variable mineralogy from sample to sample. Unmetamorphosed trials were conducted at flow rates of 1 and 2 ml/min for both samples UU and WU, and order of magnitude differences are present for the rate of solute release for trials WU1 and WU2, but not for unweathered sample UU1 and UU2. Sample UU contains a much larger percentage of quartz than any other sample, coinciding with overall lower rates of solute release and resistance to weathering.

Mancos shale mineral composition is impacted by exposure to contact metamorphism. Rock mineralogy, weatherablity and extent of metamorphism in turn control mineral reaction and chemical weathering rates, impacting landscape formation, elemental cycling, river chemistry and weathering rates within a catchment (F. Salehikhoo, et al., 2015). Compositional differences in the bulk mineralogy of metamorphosed samples compared to unmetamorphosed samples are likley linked to differences in the steady state release of solutes in metamorphosed samples compared to unmetamorphosed samples.

REFERENCES CITED

Aarnes I, Svensen H, Connolly JAD, Podladchikov YY (2010) How contact metamorphism can trigger global climate changes: Modeling gas generation around igneous sills in sedimentary basins. Geochimica et Cosmochimica Acta 74:7179–7195. doi: 10.1016/j.gca.2010.09.011

Anbeek C. (1992) Surface roughness of minerals and implications fordissolution studies. Geochim. Cosmochim. Acta 56, 1461–1469.

Atchley AL, Navarre-Sitchler AK, Maxwell RM (2014a) The effects of physical and geochemical heterogeneities on hydro-geochemical transport and effective reaction rates. Journal of Contaminant Hydrology 165:53–64. doi: 10.1016/j.jconhyd.2014.07.008

Atchley AL, Navarre-Sitchler AK, Maxwell RM (2014b) The effects of physical and geochemical heterogeneities on hydro-geochemical transport and effective reaction rates. Journal of Contaminant Hydrology 165:53–64. doi: 10.1016/j.jconhyd.2014.07.008

Babechuk MG, Widdowson M, Kamber BS (2014) Quantifying chemical weathering intensity and trace element release from two contrasting basalt profiles, Deccan Traps, India. Chemical Geology 363:56–75. doi: 10.1016/j.chemgeo.2013.10.027

Banwart S, Zhang C, Evans K (2004) Resolving the scale dependency in laboratory and field weathering rates. In: Water Rock Interaction: Proceedings of the Eleventh International Symposium on Water-Rock Interaction. Taylor and Francis Group, pp 1443–1446

Barber II, L.B., Thurman, E.M., Runnells, D.D., 1992. Geochemical heterogeneity and a sand and gravel aquifer: effect of sediment mineralogy and particle size on the sorption of chlorobenzenes. J. Contam. Hydrol. 9, 35–54.

Beckingham LE, Mitnick EH, Steefel CI, et al (2016) Evaluation of mineral reactive surface area estimates for prediction of reactivity of a multi-mineral sediment. Geochimica et Cosmochimica Acta 188:310–329. doi: 10.1016/j.gca.2016.05.040

Bluth GJ, Kump LR (1994) Lithologic and climatologic controls of river chemistry. Geochimica et Cosmochimica Acta 58:2341–2359.

Boano F, Revelli R, Ridolfi L (2007) Bedform-induced hyporheic exchange with unsteady flows. Advances in Water Resources 30:148–156. doi: 10.1016/j.advwatres.2006.03.004

Brandt, D. Bosbach, E. Krawczyk-Bärsch, T. Arnold, G. Bernhard. Chlorite dissolution in the acid pH-range: a combined microscopic and macroscopic approachGeochim. Cosmochim. Acta, 67 (2003), pp. 1451-1461

Brantley SL, Kubicki JD, White AF (eds) (2008) Kinetics of water-rock interaction. Springer Verlag, New York

Brindley, G.W. (1980) Quantitative analysis of clay mixtures. Pp. 411-438 in: Crystal Structures of Clay Minerals and their X-ray Identification (G.W. Brindley and G. Brown, editors). Monograph 5, Mineralogical Society, London.

Cerling TE, Pederson BL, Von Damm KL (1989) Sodium-calcium ion exchange in the weathering of shales: Implications for global weathering budgets. Geology 17:552. doi: 10.1130/0091-7613(1989)017<0552:SCIEIT>2.3.CO;2

Chalmers GRL, Bustin RM (2015) Porosity and pore size distribution of deeply-buried fine-grained rocks: Influence of diagenetic and metamorphic processes on shale reservoir quality and exploration. Journal of Unconventional Oil and Gas Resources 12:134–142. doi: 10.1016/j.juogr.2015.09.005

Clow DW, Drever JI (1996) Weathering rates as a function of flow through an alpine soil. Chemical Geology 132:131–141.

De Assis TA, Aarão Reis FDA (2018) Dissolution of minerals with rough surfaces. Geochimica et Cosmochimica Acta 228:27–41. doi: 10.1016/j.gca.2018.02.026

De Baere B, Molins S, Mayer KU, François R (2016) Determination of mineral dissolution regimes using flow-through time-resolved analysis (FT-TRA) and numerical simulation. Chemical Geology 430:1–12. doi: 10.1016/j.chemgeo.2016.03.014

Dere AL, White TS, April RH, et al (2013) Climate dependence of feldspar weathering in shale soils along a latitudinal gradient. Geochimica et Cosmochimica Acta 122:101–126. doi: 10.1016/j.gca.2013.08.001

Evans KA, Banwart SA (2006) Rate controls on the chemical weathering of natural polymineralic material. I. Dissolution behaviour of polymineralic assemblages determined using batch and unsaturated column experiments. Applied Geochemistry 21:352–376. doi: 10.1016/j.apgeochem.2005.10.001

Gardner CB, Carey AE, Lyons WB, et al (2017) Molybdenum, vanadium, and uranium weathering in small mountainous rivers and rivers draining high-standing islands. Geochimica et Cosmochimica Acta 219:22–43. doi: 10.1016/j.gca.2017.09.012

Gruber C, Zhu C, Georg RB, et al (2014) Resolving the gap between laboratory and field rates of feldspar weathering. Geochimica et Cosmochimica Acta 147:90–106. doi: 10.1016/j.gca.2014.10.013

Heidari P, Li L, Jin L, et al (2017a) A reactive transport model for Marcellus shale weathering. Geochimica et Cosmochimica Acta 217:421–440. doi: 10.1016/j.gca.2017.08.011

Horton TW, Chamberlain CP, Fantle M, Blum JD (1999) Chemical weathering and lithologic controls of water chemistry in a high-elevation river system: Clarks Fork of the Yellowstone River, Wyoming and Montana. Water Resources Research 35:1643–1655. doi: 10.1029/1998wr900103

Hunt AG, Ghanbarian B, Skinner TE, Ewing RP (2015) Scaling of geochemical reaction rates via advective solute transport. Chaos: An Interdisciplinary Journal of Nonlinear Science 25:075403. doi: 10.1063/1.4913257

Ilgen AG, Heath JE, Akkutlu IY, et al (2017) Shales at all scales: Exploring coupled processes in mudrocks. Earth-Science Reviews 166:132–152. doi: 10.1016/j.earscirev.2016.12.013

Jin Z, Firoozabadi A (2016) Phase behavior and flow in shale nanopores from molecular simulations. Fluid Phase Equilibria 430:156–168. doi: 10.1016/j.fluid.2016.09.011

Jin L, Ogrinc N, Yesavage T, et al (2014) The CO 2 consumption potential during gray shale weathering: Insights from the evolution of carbon isotopes in the Susquehanna Shale Hills critical zone observatory. Geochimica et Cosmochimica Acta 142:260–280. doi: 10.1016/j.gca.2014.07.006

Jin L, Ravella R, Ketchum B, et al (2010) Mineral weathering and elemental transport during hillslope evolution at the Susquehanna/Shale Hills Critical Zone Observatory. Geochimica et Cosmochimica Acta 74:3669–3691. doi: 10.1016/j.gca.2010.03.036

Jung H, Navarre-Sitchler A (2018) Physical heterogeneity control on effective mineral dissolution rates. Geochimica et Cosmochimica Acta 227:246–263. doi: 10.1016/j.gca.2018.02.028

Kaszuba J, Yardley B, Andreani M (2013) Experimental Perspectives of Mineral Dissolution and Precipitation due to Carbon Dioxide-Water-Rock Interactions. Reviews in Mineralogy and Geochemistry 77:153–188. doi: 10.2138/rmg.2013.77.5

Köhler SJ, Bosbach D, Oelkers EH (2005) Do clay mineral dissolution rates reach steady state? Geochimica et Cosmochimica Acta 69:1997–2006. doi: 10.1016/j.gca.2004.10.015

Li X, Wang Q, Zhang W, Yin H (2016) Contact metamorphism of shales intruded by a granite dike: Implications for shale gas preservation. International Journal of Coal Geology 159:96–106. doi: 10.1016/j.coal.2016.03.016

Liao X, Chigira M, Matsushi Y, Wu X (2014b) Investigation of water–rock interactions in Cambrian black shale via a flow-through experiment. Applied Geochemistry 51:65–78. doi: 10.1016/j.apgeochem.2014.09.012

Liermann LJ, Mathur R, Wasylenki LE, et al (2011) Extent and isotopic composition of Fe and Mo release from two Pennsylvania shales in the presence of organic ligands and bacteria. Chemical Geology 281:167–180. doi: 10.1016/j.chemgeo.2010.12.005

Luttge A, Arvidson RS, Fischer C (2013) A Stochastic Treatment of Crystal Dissolution Kinetics. Elements 9:183–188. doi: 10.2113/gselements.9.3.183

Ma L, Teng F-Z, Jin L, et al (2015) Magnesium isotope fractionation during shale weathering in the Shale Hills Critical Zone Observatory: Accumulation of light Mg isotopes in soils by clay mineral transformation. Chemical Geology 397:37–50. doi: 10.1016/j.chemgeo.2015.01.010

Ma L, Taylor KG, Dowey PJ, et al (2017) Multi-scale 3D characterisation of porosity and organic matter in shales with variable TOC content and thermal maturity: Examples from the Lublin and Baltic Basins, Poland and Lithuania. International Journal of Coal Geology 180:100–112. doi: 10.1016/j.coal.2017.08.002

Maher K (2011) The role of fluid residence time and topographic scales in determining chemical fluxes from landscapes. Earth and Planetary Science Letters 312:48–58. doi: 10.1016/j.epsl.2011.09.040

Matamoros-Veloza A, Newton RJ, Benning LG (2011b) What controls selenium release during shale weathering? Applied Geochemistry 26:S222–S226. doi: 10.1016/j.apgeochem.2011.03.109

May HM, Klnniburgh DG, Helmke PA, Jackson ML (1986) Aqueous dissolution, solubilities and thermodynamic stabilities of common aluminosilicate clay minerals: Kaolinite and smectites. Geochimica et Cosmochimica Acta 50:1667–1677.

Mayo AL, Loucks MD. Solute and isotopic geochemistry and ground water flow in the central Wasatch Range, Utah. Journal of Hydrology. 1995;172(1–4):31–59.

Milliken, 2004. Late diagenesis and mass transfer in sandstone-shale sequences. F.T. Mackenzie, H.D. Holland, K.K. Turekian (Eds.), Treatise on Geochemistry: Sediments, Diagenesis and Sedimentary rocks, 7, Elsevier, New York (2004), pp. 159-190

Moore, D.M. and Reynolds, R.C., Jr. (1997) X-ray Diffraction and the Identification and Analysis of Clay Minerals. Oxford University Press, Oxford, 378 pp.

Murata KJ, Dibblee Jr. TW, Drinkwater JL (1979) Thermal effects of large bodies of intrusive serpentinite on overlying Monterey Shale, southern Diablo Range, Cholame area, California.

M.C. Hidalgo, J. Groundwater composition, hydrochemical evolution and mass transfer in a regional detrital aquifer (Baza basin, southern Spain)Cruz-SanjuliaÂ n / Applied Geochemistry 16 (2001) 745±758

Nadeau PH, Reynolds RC (1981) Burial and contact metamorphism in the Mancos Shale. Clays and Clay Minerals 29:249–259.

Navarre-Sitchler A, Brantley S (2007) Basalt weathering across scales. Earth and Planetary Science Letters 261:321–334. doi: 10.1016/j.epsl.2007.07.010

Navarre-Sitchler AK, Cole DR, Rother G, et al (2013) Porosity and surface area evolution during weathering of two igneous rocks. Geochimica et Cosmochimica Acta 109:400–413. doi: 10.1016/j.gca.2013.02.012

Navarre-Sitchler A, Steefel CI, Sak PB, Brantley SL (2011) A reactive-transport model for weathering rind formation on basalt. Geochimica et Cosmochimica Acta 75:7644–7667. doi: 10.1016/j.gca.2011.09.033

Neaman A, Chorover J, Brantley SL (2004) Effects of organic ligands on granite dissolution in batch experiments at pH 6. American Journal of Science 306:451–473.

Oh YS, Jo HY, Ryu J-H, Kim G-Y (2017) A microfluidic approach to water-rock interactions using thin rock sections: Pb and U sorption onto thin shale and granite sections. Journal of Hazardous Materials 324:373–381. doi: 10.1016/j.jhazmat.2016.10.071

Petsch, S. T., R. A. Berner, and T. I. Eglinton (2000), A field study of the chemical weathering of ancient sedimentary organic matter, Org. Geo- chem., 31, 475–487.

Přikryl J, Jha D, Stefánsson A, Stipp S (2017) Mineral dissolution in porous media: An experimental and modeling study on kinetics, porosity and surface area evolution. Applied Geochemistry 87:57–70. doi: 10.1016/j.apgeochem.2017.05.004

Reeves D, Rothman DH (2013) Age dependence of mineral dissolution and precipitation rates: AGE DEPENDENCE OF RATES. Global Biogeochemical Cycles 27:906–919. doi: 10.1002/gbc.20082

Revil A (2004) Constitutive equations for ionic transport in porous shales. Journal of Geophysical Research. doi: 10.1029/2003JB002755

Riebe CS, Kirchner JW, Finkel RC (2004) Erosional and climatic effects on long-term chemical weathering rates in granitic landscapes spanning diverse climate regimes. Earth and Planetary Science Letters 224:547–562. doi: 10.1016/j.epsl.2004.05.019

Rimstidt JD, Chermak JA, Schreiber ME (2017) Processes that control mineral and element abundances in shales. Earth-Science Reviews 171:383–399. doi: 10.1016/j.earscirev.2017.06.010

Ruiz-Agudo E, Putnis CV, Putnis A (2014) Coupled dissolution and precipitation at mineral–fluid interfaces. Chemical Geology 383:132–146. doi: 10.1016/j.chemgeo.2014.06.007

Salehikhoo F, Li L, Brantley SL (2013) Magnesite dissolution rates at different spatial scales: The role of mineral spatial distribution and flow velocity. Geochimica et Cosmochimica Acta 108:91–106. doi: 10.1016/j.gca.2013.01.010

Senger K, Planke S, Polteau S, et al (2014) Sill emplacement and contact metamorphism in a siliciclastic reservoir on Svalbard, Arctic Norway. Norwegian Journal of Geology/Norsk Geologisk Forening 94:

Swoboda-Colberg NG, Drever JI (1993) Mineral dissolution rates in plot-scale field and laboratory experiments. Chemical Geology 105:51–69

Tellinghuisen J (2001) Statistical Error Propagation. The Journal of Physical Chemistry A 105:3917–3921. doi: 10.1021/jp003484u

Tuttle MLW, Fahy JW, Elliott JG, et al (2014a) Contaminants from Cretaceous black shale: I. Natural weathering processes controlling contaminant cycling in Mancos Shale, southwestern United States, with emphasis on salinity and selenium. Applied Geochemistry 46:57–71. doi: 10.1016/j.apgeochem.2013.12.010

Tuttle MLW, Fahy JW, Elliott JG, et al (2014b) Contaminants from Cretaceous black shale: I. Natural weathering processes controlling contaminant cycling in Mancos Shale, southwestern United States, with emphasis on salinity and selenium. Applied Geochemistry 46:57–71. doi: 10.1016/j.apgeochem.2013.12.010

van der Zee, S.E.A.T.M., van Remsdijk, W.H., 1991. Transport of reactive solute in spatially variable soil systems. Water Resour. Res. 23 (11), 2059–2069.

Velbel MA, Price JR (2007) Solute geochemical mass-balances and mineral weathering rates in small watersheds: Methodology, recent advances, and future directions. Applied Geochemistry 22:1682–1700. doi: 10.1016/j.apgeochem.2007.03.029

Weimer, R. J. (1960) Upper Cretaceous stratigraphy, Rocky Mountain area: Amer. Assoc. Petrol. Geol. Bull. 44, 1-20

White AF (2002) Determining mineral weathering rates based on solid and solute weathering gradients and velocities: application to biotite weathering in saprolites. Chemical Geology 190:69–89.

Williams MW, Hood E, Molotch NP, et al (2015) The "teflon basin" myth: hydrology and hydrochemistry of a seasonally snow-covered catchment. Plant Ecology & Diversity 8:639–661. doi: 10.1080/17550874.2015.1123318

Winnick MJ, Carroll RWH, Williams KH, et al (2017) Snowmelt controls on concentration-discharge relationships and the balance of oxidative and acid-base weathering fluxes in an alpine catchment, East River, Colorado: ACID-BASE VERSUS OXIDATIVE WEATHERING FLUXES. Water Resources Research 53:2507–2523. doi: 10.1002/2016WR019724